

# Blast Densification: Multi-Instrumented Case History

Guillermo A. Narsilio<sup>1</sup>; J. Carlos Santamarina<sup>2</sup>; Tamara Hebler<sup>3</sup>; and Robert Bachus<sup>4</sup>

**Abstract:** A comprehensive blast densification field study was conducted at a test site in South Carolina to densify a loose soil layer at a depth between  $z=8-13$  m. The study included extensive laboratory and field characterizations and four carefully monitored blast events. Results revealed that densification is not an instantaneous phenomenon; underlying time-dependent processes involve resedimentation, drainage of excess pore pressure as the granular skeleton deforms and the effective stress recovers, and secondary settlement effects, which do not involve excess pore pressure dissipation. The degree of densification decreased in successive blasting events, and the soil gradually evolved toward an asymptotical terminal density associated with blast densification. The blasting sequence and detonation delays appeared to have a minor effect on shear-induced movements. The increase in penetration resistance manifested 2 years after four blasting-drainage events. Instead, surface settlement using standard surveying techniques, subsurface deformation assessment, and subsurface pore fluid pressure monitoring provided valuable, real-time indicators of the soil response to the blasting events.

**DOI:** 10.1061/(ASCE)GT.1943-5606.0000023

**CE Database subject headings:** Blasting; Soil stabilization; Settlement; Measurement; Soil liquefaction; South Carolina.

## Introduction

Blast densification, also known as explosive densification, explosive compaction, or deep blasting, has been used to densify loose, saturated, sandy soils since the middle 1930s (Gnadh et al. 1999; Hall 1962; La Fosse 2002; Prugh 1963; Raju and Gudehus 1994; Solymar 1984; Wild 1961). Blasting does not require special construction machinery, and previous case histories show its effectiveness for deep compaction of uncemented granular deposits over large areas. Applications involve dam sites in Canada, India, Nigeria, Pakistan, and the U.S. (Hall 1962; Lyman 1942; Solymar 1984), transmission towers (Wild 1961), thermal power plants (Gnadh et al. 1999), airport-related projects (Fordham et al. 1991; La Fosse 2002), mines (Raju and Gudehus 1994), offshore platforms and man-made islands (Jefferies and Rogers 1993; Rogers et al. 1990), as well as liquefaction and earthquake experiments (Al-Qasimi et al. 2005; Ashford et al. 2004; Byrne et al. 2000; Robertson et al. 2000).

Typically, blast densification is used when the relative density is less than  $D_R \leq 50-60\%$ . Best results are obtained in saturated soils that are free draining. Clay content must be less than 5–10% and silt content less than 70–80% to facilitate destructuring the

soil fabric and subsequent drainage (Hachey et al. 1994; Narin van Court and Mitchell 1994).

The large energy release from the blasting creates a radial shock wave that causes initial compression in the soil mass, immediately followed by the rarefaction wave front (Charlie et al. 1985; Dowding and Hryciw 1986; Narin van Court and Mitchell 1998). The repetition of compression and extension cycles, the emergence of shear due to mode conversion at free boundaries and at interfaces in heterogeneous soil masses, and shear flow in the sediment associated with gas expansion and escape cause the increase in pore water pressure, which typically reaches the overburden pressure, i.e., a zero effective stress state. Particles resediment, a new granular skeleton is formed, and further compression takes place as the effective stress is regained (Mitchell 1981; Narin van Court 1997).

Densification is expected in initially loose sandy deposits. In particular, good to very good densification is attained when  $q_t < 10$  MPa, fair to good densification is achieved when  $q_t < 15$  MPa, and soils with CPT tip resistance  $q_t > 20$  MPa tend to loosen during blasting (Narin van Court 2003).

Settlement takes place soon after blasting and it can reach 2–10% of the treated layer thickness. The penetration resistance increases in most cases, sometimes by 50–200%; however, no increase in penetration resistance may be observed for weeks or even months after blasting (Ivanov 1983; Narin van Court and Mitchell 1998).

Design criteria for blast densification projects have developed primarily from experience rather than from theoretical analyses. The main design variables include: (1) mass or weight of explosives per  $m^3$  of sediment; (2) charge distribution, i.e., spacing and pattern of boreholes, depth of explosives, and vertical distribution of charges within boreholes; (3) number of events; (4) blasting sequence; and (5) delay time. Semiempirical guidelines are summarized in Table 1.

While large charges affect a large volume, they do not necessarily increase densification (obviously, charges should not be too large to cause surface blow up); instead, sequential detonation-and-drainage cycles of more closely spaced small charges can be more effective (Terzaghi et al. 1996). Furthermore, there is some

<sup>1</sup>Research Fellow, Dept. of Civil and Environmental Engineering, The University of Melbourne, Civil Engineering Block D 317, Parkville, VIC 3010, Australia. E-mail: narsilio@unimelb.edu.au

<sup>2</sup>Professor, School of Civil and Environmental Engineering, Georgia Institute of Technology, 790 Atlantic Dr., Atlanta, GA 30332-0355. E-mail: jcs@gatech.edu

<sup>3</sup>Senior Engineer, Geosyntec Consultants Inc., 1255 Roberts Blvd., Ste. 200, Kennesaw, GA 30144. E-mail: THebler@Geosyntec.com

<sup>4</sup>Principal Engineer, Geosyntec Consultants Inc., 1255 Roberts Blvd., Ste. 200, Kennesaw, GA 30144. E-mail: RBachus@Geosyntec.com

Note. This manuscript was submitted on September 25, 2007; approved on September 10, 2008; published online on February 19, 2009. Discussion period open until November 1, 2009; separate discussions must be submitted for individual papers. This paper is part of the *Journal of Geotechnical and Geoenvironmental Engineering*, Vol. 135, No. 6, June 1, 2009. ©ASCE, ISSN 1090-0241/2009/6-723-734/\$25.00.

**Table 1.** Blast Densification—Design

Charge size	Depth	Horizontal spacing	Detonation interval	Detonation sequence	Number of events	Related observations	References
$M=0.10 \times z_w^{2.46}$	$1.8 \cdot M^{1/3}$	$s=4 \cdot M^{1/3}$					Ivanov (1967)
1–12 kg 8–850 gr/m <sup>3</sup> 10–30 gr/m <sup>3</sup>	$> \frac{1}{4}$ depth to bottom of layer to be treated (usually $\frac{1}{2} - \frac{3}{4}$ )	5–15 m	Hours to days		1–5 (usually 2–3)	$\Delta S=0.02H$ to $0.10H$	Mitchell (1981)
3.6 kg (30% special gelatin dynamite)	3, 6, and 11 m	6 m	4 h			Porosity changed from 47 to 43% at Karnafuli Dam ( $D_{10}=0.18$ mm, $C_u=2$ )	Terzaghi et al. (1996)
$HN=M^{1/3}/R$	$R$ or $\frac{2}{3}$ depth to bottom of layer to be treated	$R$	Preliminary test needed	From the edges, inwards (Polish experience)		$\Delta S=H[2.73+0.9 \ln(HN)]$	Ivanov (1967) van Impe (1989) Narin van Court and Mitchell (1998) Narin van Court (1997, 2003)
$NM=\frac{(M/L_c)^{1/2}}{R}$	$H_B=1.48 \cdot Q^{1/2}$ $H_1=2.63 \cdot C^{1/3}$	Square or equilateral triangles				May not be valid for different patterns and site conditions	Dembicki et al. (1992) Imiolek (1992) Narin van Court and Mitchell (1998) Narin van Court (2003)
$E_1=\sum \left( \frac{M_i}{R_{vi}^2} \right)$ with $350 < E_1 < 3,500$	Layers $>7-8$ m should be divided in sublayers of 5–6 m thick	Square grid 4.5–11 m (preferably, 4.5–6 m) $s=1.4 \cdot s_{\text{final}}$ $s=2 \cdot s_{\text{final}}$ (in the first two events if three events are needed)	Several min (controlled by $u$ -dissipation)	Outward, from center to outside	1–3	Predicted final $q_t$ in CPT: $q_{1,f}=0.195 \cdot q_0^{0.478} \cdot E_1^{0.330} \cdot \sigma_v'^{0.175}$ ( $R^2=0.66$ ) $q_{1,f}=0.404 \cdot q_{1,0}^{0.525} \cdot E_1^{0.327}$ ( $R^2=0.64$ )	Narin van Court (2003)

Note:  $M$  explosive charge mass (kg),  $z_w$  ground water table depth,  $\Delta S$  surface settlement (m),  $H$  thickness of the layer treated by blast densification, recommended Hopkinson's number values [as defined by Ivanov (1967)]  $HN$ : 0.15 (van Impe 1989), 0.50 (Narin van Court 2003), 0.2–0.5 (Ivanov 1967), 0.5–1.2 for nonconcentrated charges (Ivanov 1967), or chose  $HN$  such that  $M=10$  kg TNT (Ivanov 1983),  $R$  effective radius in plan (m) =  $1/2 \cdot s$ ,  $s$  grid spacing, recommended normalized explosive charge mass values [as defined by Dembicki et al. (1992)]  $NM$ : 0.3–0.6 (Dembicki et al. 1992), 0.4–0.7 (Narin van Court 2003),  $H_b$  minimum distance from ground surface to top of charge (m),  $Q$  charge loading density (in kg/m),  $C$  concentrated charge (kg). Recommended energy input attenuation  $E_1$  values at the center of the grid using  $M_i=4-7$  kg per sublayer, depending on spacing:  $350 < E_1 < 1,000$  for very loose soils ( $q_t < 5$  MPa),  $1,500 < E_1 < 3,500$  for loose to medium soils ( $5 \text{ MPa} < q_t < 15 \text{ MPa}$ ) or  $750 < E_1 < 1,500$  for two events, with no mayor dependency on  $\sigma_v'$ ,  $R_{vi}$  minimum distance from charge to a point in the soil mass (in m),  $q_{1,f}$  CPT final normalized tip resistance,  $q_t$  CPT tip resistance.

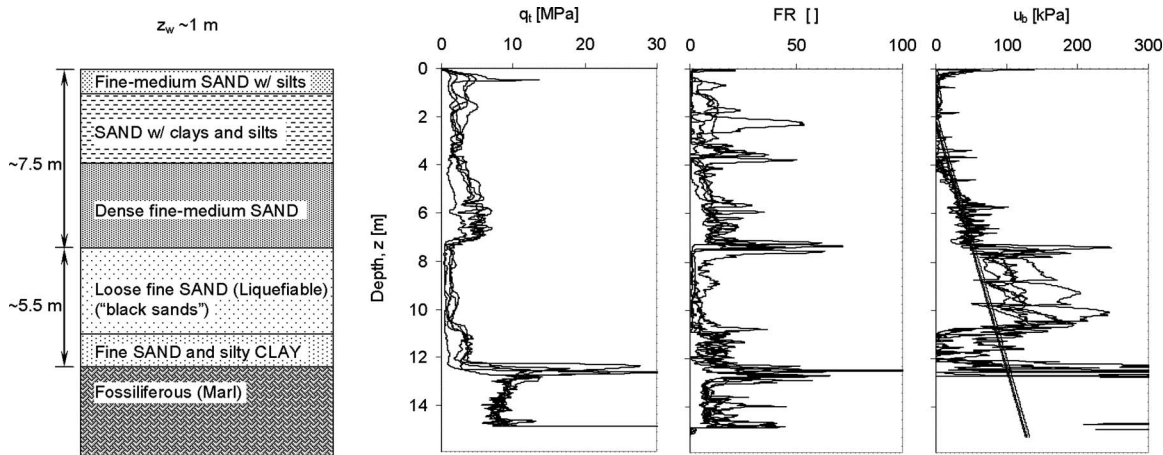


Fig. 1. Representative soil profile; before-blasting-CPT profiles at different locations within the site are shown

evidence that densification may be increased when a second set of charges is detonated in a previously blasted sediment while the pore water pressure is still elevated (Ivanov 1983; Minaev 1993); in this case, the initially low shear resistance facilitates vibration-induced compaction.

The upper 1–3 m thick soil layer may be loosened because of the upward seepage forces of the escaping fluids and blast-induced deformations. Furthermore, sand boils spread a loose layer of fine sand and silt across the surface. Therefore, the upper layers may require postblasting compaction. Alternatively, a temporary 3 m thick layer of gravel can be placed on the surface to mitigate these near-surface effects (Narin van Court 2003).

In this manuscript, we document a blast densification case history that involved extensive laboratory and field characterization, and four carefully monitored blasting events. Data, analyses, and lessons learned follow. The complete study can be found in Narisilio (2006).

### Test Site Description—Soil Properties

The test site is located in South Carolina. The formation consists of a relatively new deposit on the coastal geological province (pleistocene—quaternary). There are six distinguishable layers (Fig. 1): unsaturated near-surface sands ( $z=0$  to  $z\cong 0.6$  m below ground surface); sand layers with some silt and clay ( $z=0.6$  m to  $z\cong 4.0$ – $6.0$  m); fine and clean white sand ( $z\cong 4.0$ – $6.0$  to  $7.3$ – $7.5$  m); loose, very fine “black sand” on top of a thin denser fine sand and silty clay horizon ( $z\cong 7.5$  m to  $z\cong 10.7$ – $13.0$  m); and a greenish/olive-gray fossiliferous marl layer ( $z > \sim 13.0$  m). The water table is at  $z_w=0.8$ – $1.5$  m below the surface.

A comprehensive laboratory and field characterization program was implemented to evaluate all layers, with emphasis on the loose fine sands encountered between the nominal depths  $z=8$ – $13$  m throughout the site. The study encompassed index properties, hydraulic conductivity, consolidation, small strain stiffness, strength, and geophysical properties. Results are summarized in Tables 2 and 3.

The blast densification program was targeted to the loose sandy layer between  $z=8$ – $13$  m. An initial  $18.3$  m  $\times$   $18.3$  m area was selected for this purpose (Fig. 2—dashed lines). The blast design was based on guidelines listed in Table 1. Four blasting events were implemented in a period of more than 8 months.

They involved individual explosive charges ranging from 11 to 34 kg placed at  $z=10$  m in a square grid pattern with a fixed spacing of approximately 9 m. Fig. 2 shows the aerial distribution of charges for the four blasting events (relevant details are included in Table 4). Note that while delay times were 10 and 50 ms in the first and second blasting events, a delay of 10 min was used in the third and fourth blasting events to test the advantages of vibrating soil with already high pore pressure, i.e., by initiating the next detonation before the high excess pore pressures have dissipated.

Explosives were installed in predrilled and PVC-encased boreholes [Fig. 3(a)]. The explosive (Hydromite 860—powder factor  $0.067$  lb/yard<sup>3</sup> or  $39.7$  grams/m<sup>3</sup>) was lowered to the desired “central” depth ( $z=10$  m; the charge varied from 0.8 to almost 2.3 m long). The rest of the borehole was then back-filled with gravel.

### Field Measurements

A thorough monitoring program was implemented to gain extensive information before, during, and after each of the four blast events. The monitoring program included: (1) ground surface settlement using standard surveying equipment; (2) subsurface settlements using three Sondex systems S1, S2, and S3 (Fig. 2); (3) vibration assessment using surface geophones and a 12 channel seismograph; (4) CPTu penetration studies; (5) ground penetrating radar GPR; and (6) pore-water pressure using two vibrating wire piezometers P1 and P2 (Fig. 2). The following section presents representative results and summarizes the most important observations.

#### Surface Settlement

Standard topographic surveys were conducted before, during, and after each of the blasting events. The evolution of cumulative surface settlement in time along the N-S center line is shown in Fig. 4. The four thicker lines show the maximum recorded settlement a month or more after each blast event. The vertical lines indicate the position of the outside rows of explosives in each event (refer to Fig. 2).

The affected surface extended a distance similar to the blasting depth outside the blasting zone in each direction. A detailed analysis of the complete survey data reveals that the surface

**Table 2.** Soil Parameters and Index Properties—All Horizons

Depths [m]	10					
	2	4	6	Field condition	Washed	13
Classification						
#4 Passing (%)	100.0	100.0	100.0	100.0	100.0	100.0
#200 Passing (%)	0.7	1.2	0.6	0.7	3.7	2.0
$D_{60}$ (mm)	0.20	0.20	0.32	0.22	0.21	0.21
$D_{50}$ (mm)	0.19	0.19	0.29	0.21	0.19	0.20
$D_{30}$ (mm)	0.18	0.18	0.22	0.17	0.17	0.17
$D_{10}$ (mm)	0.16	0.16	0.17	0.15	0.12	0.15
$C_u$	1.25	1.25	1.88	1.47	1.75	1.40
$C_{cur}$	1.01	1.01	0.89	0.88	1.15	0.92
USCS	SP	SP	SP	SP	SP	SP
$w$ (%)	25.6	27.3	26.0		31.4	32.9
$e_0$	0.68	0.72	0.69		0.84	0.878
$\sigma_{fluid}$ [S/m] (@ 200 MHz)	0.041	0.044	0.082		1.23	0.310
Particle shape (soil retained on sieve #100)						
Sphericity				S=0.60 (average of all samples)		
Roundness				R=0.15 (average of all samples)		

Note: "Field condition" refers to disturbed specimens obtained from split barrels samplers; "washed" indicates specimens whose fines have been washed out. The initial void ratios are estimated from water content assuming complete saturation.

settlements exhibit some correlation to the location of explosives. For example, the settlement after the second blast was quite uniform in agreement with the uniform spatial distribution of charges; however, the settlement after the third and fourth blasts was more pronounced where there was a denser spatial configuration of explosives.

The incremental surface settlement decreased after each consecutive blast, from 0.16 m for the first event,  $\sim$ 0.12 m for the second and third events, and 0.09 m after the fourth event [data shown in Fig. 5(a)]. Some settlement was still observed 10 h after blasting. The evolution of cumulative surface settlement with time at the center and at a border of the  $18.3 \times 18.3$  m test area is summarized in Fig. 5(b).

### Water out of Boreholes

Fluids flowed from the top of the most recently installed blast pipes after each blast event (visual observation). Gas came out first, immediately after the blast; water flow started a few seconds later. The duration of water flow decreased with subsequent blast events: it lasted 12 h after the first blast, 4 h after the second blast, about 10 min after the third blast, and 5 min after the fourth blast. Settlement-time data and the duration of water flow point to the causal link between excess pore water pressure dissipation, settlement, and densification, which will be discussed later in the text.

### Subsurface Settlement

Subsurface settlements were monitored using a corrugated pipe with periodic metallic sensing rings. The installation of the corrugated pipe in the bentonite-stabilized boreholes required pushing down against a bottom plate fixed to the end of the corrugated pipe (note: this procedure caused the extension of the pipe and might have led to locked-in tension, which could be released during liquefaction). Fig. 3(b) shows a schematic diagram of the

installed system. Vertical deformation was measured by detecting the location of rings with a probe that is lowered into the hole.

Subsurface settlement measurements were taken at three locations (Fig. 2): outside the test area defined by the perimeter of charges S1 yet within the area of influence, at the center of the test site S2, and on the perimeter S3. Typical settlement-versus-initial depth profiles measured at different times are shown in Fig. 6. Most of the vertical deformation accumulated in the lower loose layer ( $z=8-13$  m), while the upper layers ( $z \leq 7$  m) behaved as a rigid block, i.e., ring vertical displacements and subsurface settlements were almost constant for the first  $\sim 6-7$  m. Negative settlements near the bottom may be due to heave associated with the impact of the blast front on the corrugated pipe and/or the release of tension locked in during the installation. Fig. 7 shows the cumulative contraction of the upper layer between ring #1 (initial depth  $\sim 1$  m) and ring #7 (initial depth  $\sim 7$  m), and the loose layer between ring #8 (initial depth  $\sim 8$  m) and ring #15 (initial depth  $\sim 13$  m; listed ring numbers correspond to subsurface settlement unit S3); results are shown for the three locations of the Sondex probes: outside S1, at the border of S3, and at the center of S2 of the test area. Fig. 7(b) and 5(b) show the same settlement trends and magnitudes; this confirms that most of the surface settlement [Fig. 5(b)] is due to the contraction of the loose layer (Fig. 7).

### Vibration Assessment

The vibrations caused by the explosions were measured using 3D geophones at four stations along the N-S centerline at 9, 12, 15, and 18 m away from the edge of the blast zone. Fig. 8 shows typical signatures gathered during the second blast event; the vertical motion has been low-pass filtered to recover unsaturated low frequency components and normalized to the maximum measured vertical amplitude. Most of the motion took place in the vertical  $z$  direction. The front traveled with a velocity of  $\sim 1,500$  m/s,

**Table 3.** Engineering Properties for the Shallow Cap Layer and the Deeper Loose Layer of Interest

Depth (m)	4	10 (soil of most interest)
Specific gravity, $G_s$	2.65	2.67
Minimum dry unit weight, $\gamma_{\min}$ (kN/m <sup>3</sup> )	11.93	12.50
Maximum void ratio, $e_{\max}$	1.179	1.096
Minimum void ratio, $e_{\min}$	0.54	0.52
$D_R$ (%) (estimated from water content)	71	38–44
$k$ [cm/s] (falling head)	$4 \times 10^{-5} - 6 \times 10^{-4}$	$1.5 \times 10^{-5} - 7 \times 10^{-3}$ (ASTM D5084-B)
pH		4.11 (Fisher Scientific Accumet AR50 pH Meter)
Velocity—stress trends		
$\alpha_{vs}$	36 ( $D_R=52\%$ )	45 ( $D_R=35\%$ ) 89 ( $D_R=47\%$ —oven dried) 51 ( $D_R=62\%$ )
$\beta_{vs}$	0.312 ( $D_R=52\%$ )	0.296 ( $D_R=35\%$ ) 0.234 ( $D_R=47\%$ —oven dried) 0.289 ( $D_R=62\%$ )
Critical state soil parameters		
$\Gamma$ (intercept)	1.232 1.313 1.037	1.165 (Measured) 1.205 (From $e_{\max}$ , $e_{\min}$ , and $C_u$ ) 1.037 (Estimated from $R$ and $S$ )
$\lambda$ (slope)	0.113 0.096 0.240	0.138 (Measured) 0.086 (From $e_{\max}$ and $e_{\min}$ ) 0.200 (From $\Gamma$ and $e_{\min}$ )
$\phi_{cs}$	32°	33°–40°
Oedometer		
$C_c$ (last loading stage)	0.0347 ( $D_R=52\%$ )	0.0528 ( $D_R=35\%$ ) 0.0728 ( $D_R=47\%$ —oven dried) 0.0347 ( $D_R=62\%$ )
$C_r$ (last unloading state)	0.00291 ( $D_R=52\%$ )	0.0036 ( $D_R=35\%$ ) 0.0028 ( $D_R=47\%$ —oven dried) 0.0021 ( $D_R=62\%$ )
$C_c/C_r$	16 ( $D_R=52\%$ )	15 ( $D_R=35\%$ ) 26 ( $D_R=47\%$ —oven dried) 16 ( $D_R=62\%$ )

which is compatible with the  $P$ -wave velocity for a saturated soil. Surface vibrations continued for about 0.5 sec after blasting.

Detonation delays can be identified in the seismic signatures, as shown in Fig. 9 (note: the particle motion shown in this figure takes place in the  $y$ -direction, which is parallel to the direction of energy radiation; the time scale in Fig. 9 is expanded compared to Fig. 8). Therefore, vibration monitoring can be used to verify the implementation of time delays required as part of the blasting program: the observed time delays closely matched the 50 ms delay specified for this event (Table 4). Note that delays observed in vibration record must be corrected for the relative position of the sensors with respect to each detonation.

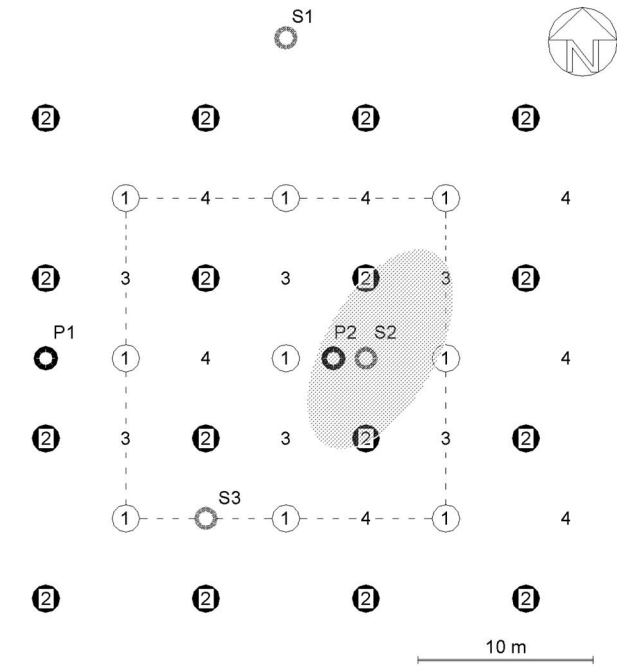
### Penetration Tests

A very extensive cone penetration testing (CPTu) program was implemented to assess the consequences of blast densification on penetration parameters, corrected tip cone resistance  $q_t$ , sleeve friction  $f_s$ , and pore water pressure  $u$ . Penetration tests were repeated throughout the test area and peripheral zones before the blasting events, as well as 19, 37, 301, 742, and 1,292 days after the first blasting event. Fig. 10 shows profiles of corrected tip resistance  $q_t$  determined within the test site (see Fig. 2), where the corrected tip resistance  $q_t = q_c + (1 - a_n)u_b$  is computed from the

measured tip cone resistance  $q_c$  taking into consideration the shoulder pore-water pressure  $u_b$  through the net area ratio  $a_n$  obtained from triaxial calibration (as per ASTM D 5778). All penetration studies showed similar results (Fig. 10): there was very limited improvement—even weakening—in penetration parameters during the first year after the blasting program started; clear improvement in penetration resistance is detected 1,292 days after the first blasting, that is 1,034 days after the fourth and last blasting event.

### Ground Penetration Radar Images

Laboratory measurements of electrical conductivity showed that the skin depth for ground penetration radar (GPR) was shorter than the depth of the loose sand layer (data in Table 2—skin depth is the distance over which the electromagnetic signal decays by  $1/e$  of its original value at the surface). Therefore, we deployed GPR in the field to assess the effect of blasting on the overlying layers rather than to monitor the evolution of the blasted layer [as in Kayen et al. (2005)]. Fig. 11 shows typical GPR profiles along the N-S centerline of the test site (a) before and (b) 20 h after a single blast event. Signals are time enhanced to compensate for spherical spreading and ohmic losses. The last measurable reflector at around 200 ns corresponds to the top of the loose



Blast Event	Date	# of charges	Individual charge	Detonation delay
○ 1 <sup>st</sup>	11/21/03	9	19 kg	100 ms between rows
● 2 <sup>nd</sup>	12/23/03	16 (+1) <sup>a</sup>	34 kg	50 ms between rows
◇ 3 <sup>rd</sup>	06/04/04	6	11 kg	10 min between rows
★ 4 <sup>th</sup>	08/05/04	7	11 kg	10 min between rows

○ P Piezometer   ○ S Subsurface settlement   - - - Initial blasting area

**Fig. 2.** Site geometry; location of the explosives (four events), piezometers (P1 and P2), and subsurface settlement systems (S1, S2 and S3); the explosives are buried ~10.0 m in depth; the shaded zone indicates the locations of CPT soundings reported in Fig. 10; a single charge is detonated first due to detonation failure of one of the charges during the first event

layer (corroborated using common midpoint measurements not shown here). While there are some minor differences among the two profiles, the general trend indicates that reflectors occur at the same times in records obtained before and after blasting; therefore, these results suggest no change in volumetric water content and confirm that sediments in the upper ~7 m settled as a rigid body in agreement with subsurface settlement data (Figs. 6 and 7).

### Pore-Water Pressure

Two vibrating wire piezometers were installed, one at the boundary of the test area defined by the perimeter of charges (P1,  $z = 10.5$  m) and the other, at the center (P2,  $z = 11.5$  m—Fig. 2). The

**Table 4.** Field Tests—Blasting Events

Blasting event	Grid	Number of charges	Individual charge (kg)	Explosive type/depth	Delay sequence detonation
First (11/21/03)	Three rows, three columns (square)	9	19	Hydromite 860/10 m	100 ms between rows
Second (12/23/03)	Four rows, four columns (square)	16 (+1) <sup>a</sup>	34	Hydromite 860/10 m	50 ms between rows
Third (06/04/04)	Two rows, three columns (square)	6	11	Hydromite 860/10 m	10 min between rows
Fourth (08/05/04)	Three rows, three columns (square)	7	11	Hydromite 860/10 m	10 min between rows

<sup>a</sup>A single charge is detonated first due to detonation failure of one of the charges during the first event.

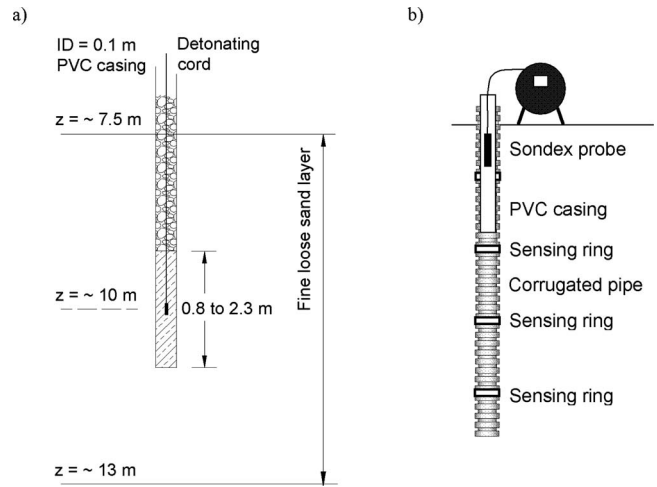


**Fig. 3.** (a) Details of explosive installation; (b) subsurface settlement; measurement of vertical strain with depth (Sondex system)

piezometers were placed inside encased boreholes (ID=25 mm, PVC pipe slotted in the bottom 1 m), which were back-filled and sealed with subsequent layers of medium sand and bentonite to ensure that pressure readings correspond to the pore pressure at the installation depths. The pore pressure was measured every 2 sec during the first hour after blasting and every 2 min thereafter (minilogger by Slope Indicator).

Data for the three detonations during the fourth blast event are plotted in Fig. 12 (this event involved relatively small charges  $M=11$  kg—Table 4). The pore pressure for full liquefaction  $u_L$  shown in the figure is equivalent to the total vertical stress, which is calculated using the total unit weight profile. The piezometer data show that a zero effective stress condition was attained at the center of the test site (P2) during the second detonation of the long-delayed sequence imposed in this event.

## Analyses and Discussion

### Settlement and Volumetric Strain

The total settlement after the four blast events was  $S \cong 0.50$  m, and corresponds to an average volumetric strain of  $\epsilon_v \cong 12\%$  in the lower layer, i.e., about 3% per blasting event (for this analysis, the lower layer between  $z=8-13$  m is considered, in agreement with GPR and subsurface settlement measurements shown in Figs. 6, 7, and 11). Estimated values for the initial in situ void ratio range between: (a)  $e_0 \cong 0.97$  obtained as  $e = e_{\max} - D_R(e_{\max} - e_{\min})$  for a relative density  $D_R \cong 12\%$  inferred from the corrected tip cone resistance  $q_t$ —see Fig. 1 and Table 3, and (b)  $e_0 \cong 0.84$  computed from water content measurements (Table 2). The de-

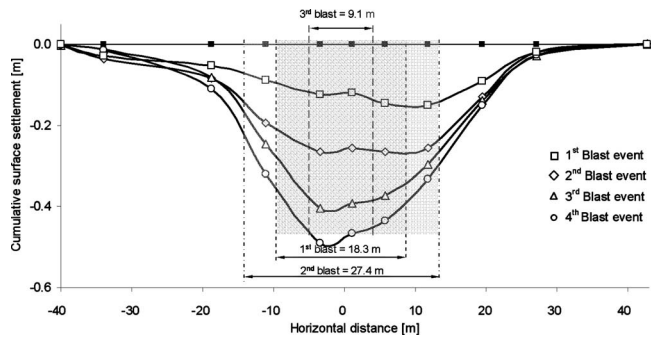


**Fig. 4.** Cumulative surface settlement; the lines correspond to the maximum recorded settlement at the end of the wait period after each blast (north-south cross section through the center of the test site— Fig. 2)

crease in void ratio then is  $\Delta e = \varepsilon_v(1 + e_0) = 0.22 - 0.24$ . This reduction in void ratio should bring the final soil void ratio into the dilative region,  $e_f \cong 0.62 - 0.73$  (the estimated critical state void ratio is  $e_{cs} \cong 0.85$  at 10 m depth), and significantly lowers the consequences of a potential seismic event. Despite the uncertainty involved in the estimation of the initial in situ void ratio and critical state parameters (Tables 2 and 3), it is safe to conclude that the densified sand layer will exhibit a higher liquefaction resistance.

The surface settlement measured in this study extended beyond the blasting area by approximately the blasting depth in

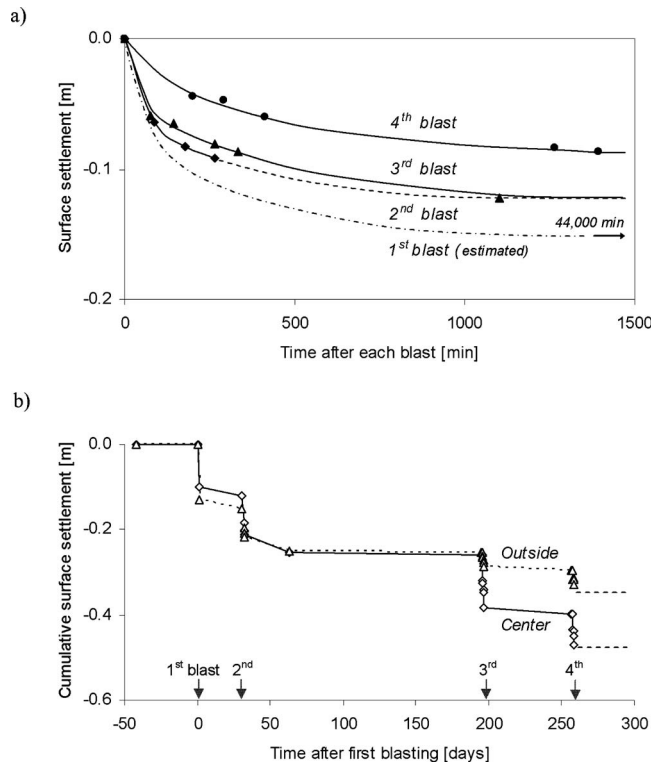


**Fig. 5.** Surface settlement versus time: (a) settlement of the ground surface versus time for the individual events; the curve for the first blast is sketched based on the measured settlement after  $t = 44,000$  min and the other trends; (b) cumulative settlement of the ground surface over time, at the center and just outside the  $18.3 \times 18.3$  m blasting area (Fig. 2)

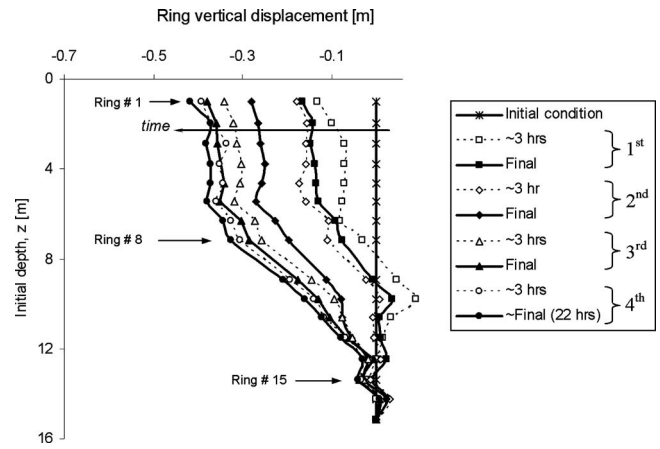


**Fig. 6.** Typical subsurface settlement measurements; the data correspond to the S3 unit (refer to Fig. 2)

each direction (Fig. 4). This observation is expected to depend on the upper layer thickness and stiffness. The comprehensive analysis of the 2D settlement data for all blast events suggest that the maximum recorded settlements after blasting were near the location of the explosives, a more uniform spatial explosive distribution caused a more uniform surface settlement, and larger settlements were measured above regions with a denser spatial configuration of explosives.

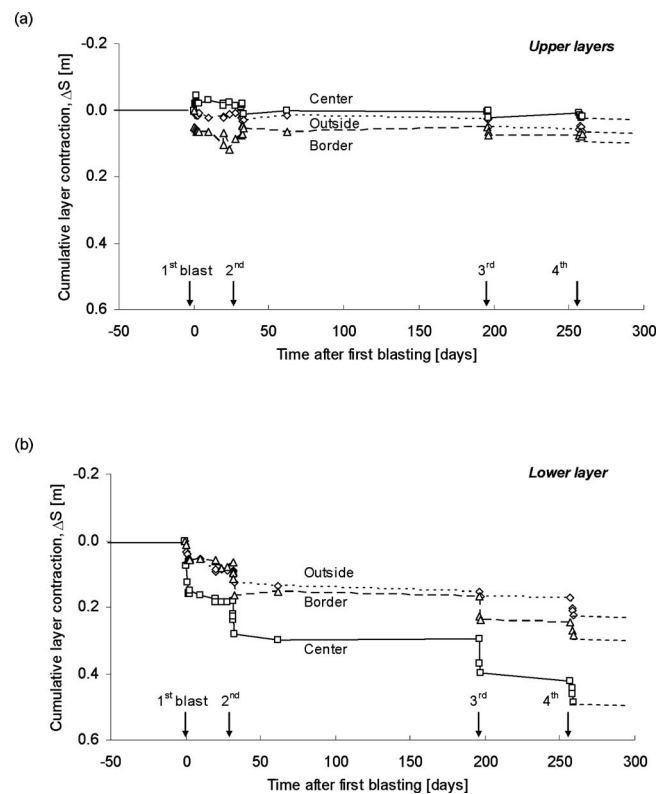


**Fig. 7.** Cumulative layer contraction as a function of time (refer to Fig. 6); the data reflect the shortening of the distance between (a) rings #1 and #7 for the upper layers; (b) rings #8 and #15 for the lower layer

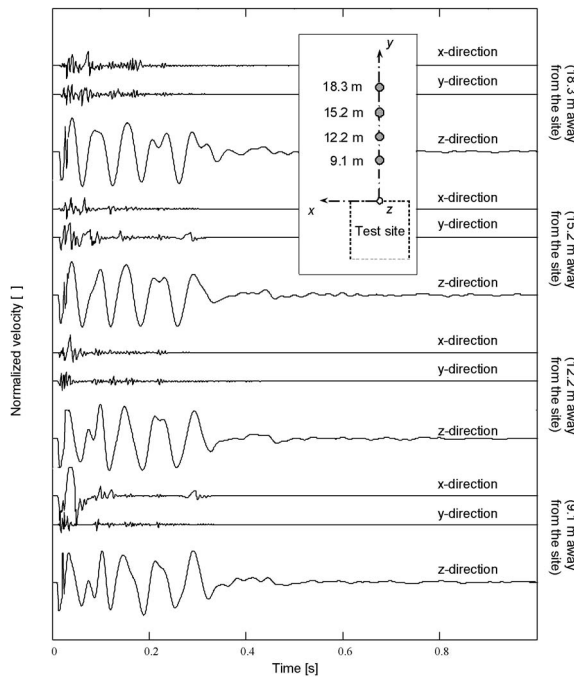


**Fig. 8.** Typical measured signals in the three directions; these records correspond to the second blast event and are normalized to the maximum measured vertical amplitude

### Vibration Analysis

Vibration data were analyzed using hodographs to investigate the extent of induced shear effects due to imposed detonation delays and sequences (hodographs are plots of particle motions in different directions:  $u_y$ -vs- $u_z$ ,  $u_x$ -vs- $u_z$ , and  $u_x$ -vs- $u_y$ —these plots are not shown here). The hodographs for a given blast event were similar at the four 3D surface geophone stations. The blasting

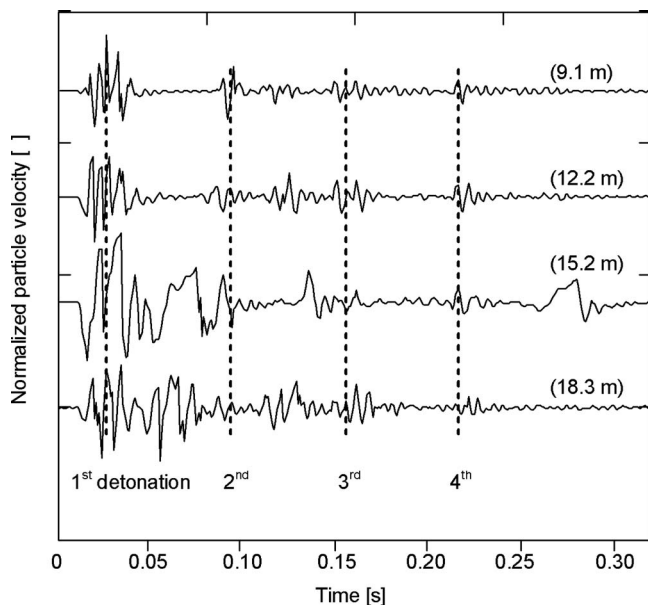


**Fig. 9.** Identification of the four detonations during the second blast event (normalized particle motion in the  $y$ -direction is shown); the designed time delay between detonations was 50 ms

sequence and delays enhanced the induced soil shearing (transverse shear in the direction of the detonation sequence) during the initial few milliseconds only.

While blasts generate an initial spherical wave, the detected motion away from the site had a very small normal component (quasi- $y$ -direction—Fig. 8). The transverse  $x$ -motion was most pronounced in the near field, and it was purposely caused by the imposed delay and blasting sequence that advanced in  $x$  for the event shown in Fig. 8. The interaction between the blast dynamics and the free surface led to energy radiation away from the source primary in the form of a surface wave, as manifested by a strong  $z$ -motion in all sensors (Fig. 8).

The ratio of vertical-to-horizontal particle motion is  $u_z/u_y \sim 0.5$ ; for comparison, the theoretical ratio in surface waves measured in the far field of sources is 0.6 for a Poisson's ratio of 0.25 (Richart et al., 1970). Albeit limited by partial saturation in recorded vertical motions, this result suggests that most of the energy was radiated along the surface in the form of  $R$ -waves even at relatively short distances from the source.

The benefits of time delays in promoting long-lasting vibration were readily noted in this study. While the sequential detonation of charges with well controlled delays could enhance the transverse movement of the upper layer and cause additional shear, the possibility of engineering the blasting sequence to enhance shear requires further numerical and field investigation. Indeed, nonlinear effects and complex vibration modes hamper simple analyses. For example, we estimated the 50 ms time delay to trigger resonance and to maximize vibration in this field study, however, records in Fig. 8 show that the fourth detonation at around 0.22 s caused destructive rather than constructive interference.

### Penetration Resistance

CPT soundings showed no evidence of soil improvement in the short term, even though the blasting program lasted 8 months, involved four blast events, caused more than 0.5 m settlement, and an estimated reduction in void ratio of  $\Delta e \sim 0.23$ . The increase in corrected tip cone resistance was finally detected more than a year after the completion of the fourth and last blast event. This is not a unique case, in fact, several blasting studies reported in the literature show that several months passed before the tip resistance reached pre-blast values (Charlie et al. 1992; Jefferies and Rogers 1993; Mitchell and Gallagher 1998). The recent review of sand aging by Mitchell (2008) provides further insight into the complexity of underlying phenomena responsible for this response (Mitchell, 2008).

Another coexisting effect is the limited sensitivity of CPT to relative density in loose sediments. This is inherently captured in the following parabolic expression that predicts relative density  $D_R$  (%) from the cone tip resistance  $q_t$  (kPa) normalized by the in situ effective vertical stress  $\sigma'_{v0}$  (kPa) (Kulhawy and Mayne 1990):

$$D_R = 1.8 \sqrt{\frac{q_t}{\sigma'_{v0} \cdot \text{kPa}}} \quad (1)$$

Based on this expression, the gathered penetration data would indicate that the initial in situ relative density for the loose sandy layer was  $D_R = 20$ – $30\%$  before blasting and increased to  $D_R \approx 40\%$  after 742 days from the first event, i.e., 484 days after the last and fourth blasting event (Fig. 10). However, robust subsurface and surface settlement measurements gathered at the same times suggest a change in void ratio  $\Delta e \sim 0.23$ , which would have brought the in situ relative density to  $D_R = 60$ – $70\%$ .

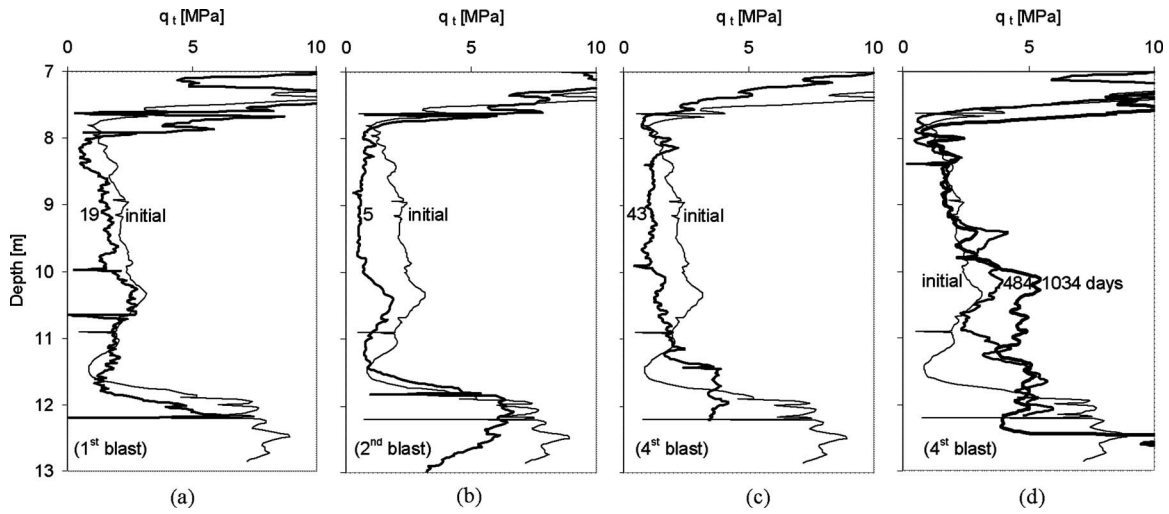


**Fig. 10.** Evolution of the CPT tip resistance  $q_t$  over time between depths 7 and 13 m; the  $q_t$  profile gathered before blasting is shown as a thin line in all panes for reference (initial); the other profiles shown as thick lines correspond to: (a) 19 days after the first blast event; (b) 5 days after the second blast event; (c) 43 days after the fourth blast event; and (d) 484 days (thick line) and 1,034 days after (thicker line) the fourth blasting; all soundings are closely located within the test site—zone shown in Fig. 2 (data gathered by G. Hebel, T. Hebel, and R. Kulasingam)

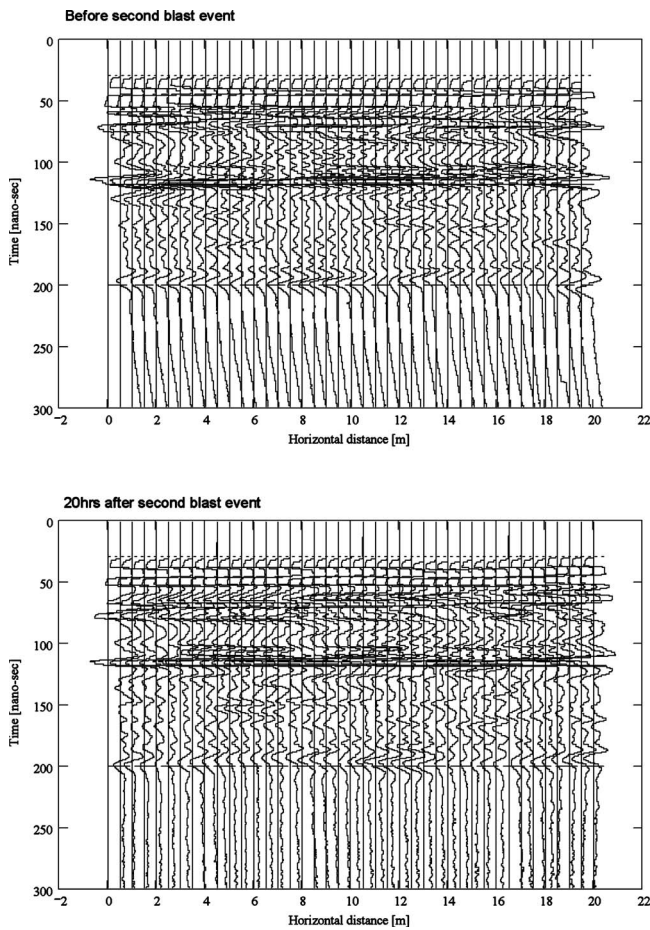


**Fig. 11.** Typical GPR profiles; the last reflection at  $\sim 200$  ns corresponds to the top of the loose sand layer (GPR with 200 MHz antennae, second blast event)

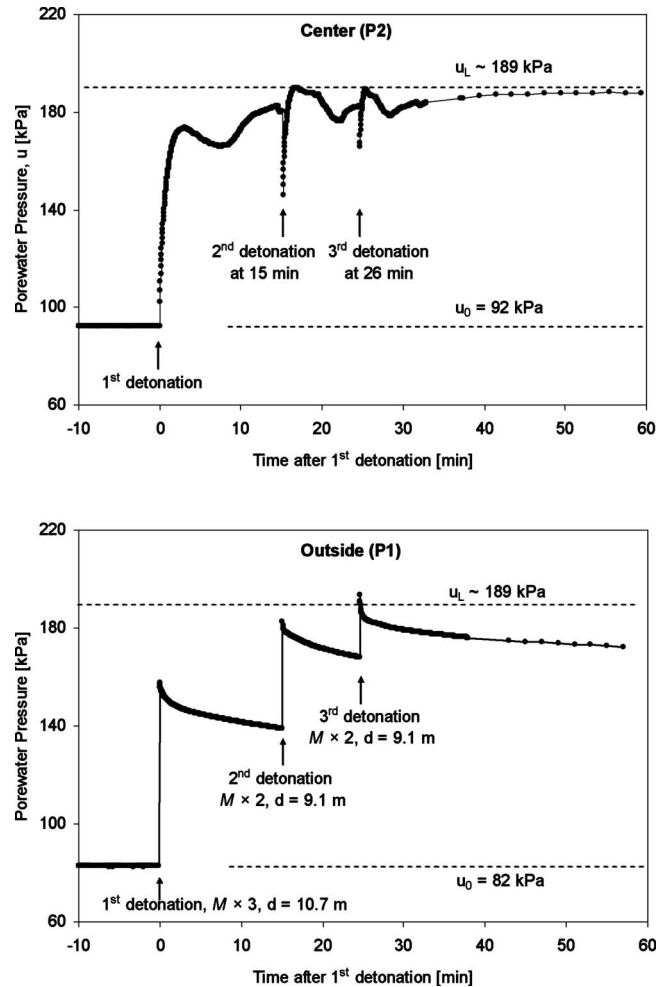


**Fig. 12.** Pore pressure measurements during the fourth blast event; the charge mass  $M$  is 11 kg for this event

### Terminal Density

Field data showed a decrease in the incremental surface settlement after each consecutive blast [0.16 m for the first event, ~0.12 m for the second and third events, and 0.09 m after the fourth event—Fig. 5(a)], and in the amount of water that escaped through borings after each blast event. These results are compatible with the concept of “terminal density” which states that every given soil eventually reaches a unique terminal density and internal fabric when subjected to repetitive events (Narsilio and Santamarina 2008).

### Rate of Settlement—Pore Pressure Dissipation

The time varying settlement and excess pore pressure dissipation are plotted in Fig. 13 for the central and peripheral locations of the test site in the field: the excess pore pressure decreased by 90% in 24 h, and approximately 86% of the total settlement took place in the same period of time. Yet, settlement and pore pressure dissipation curves do not follow identical patterns: there was a steep early settlement even at relatively constant excess pore pressure [Fig. 13(b)], and some settlement continued long after the excess pore pressure has dissipated (Figs. 4, 5, and 7). These data allow us to hypothesize the following sequence of events [refer to Lee and Santamarina (2007) for related studies]: early drainage of water and gas, resedimentation and formation of a bottom-up densification front (noted in CPT data in Fig. 10), drainage of excess pore pressure as the skeleton deforms with the increase in effective stress (i.e., consolidation), and secondary settlement effects.

The duration of the liquefied state and drainage are related to the time scale for resedimentation and excess pore-water pressure dissipation after blasting. The time scale for resedimentation and early fluid flow are estimated as follows: assuming that all the settlement  $S$  is concentrated in the lower layer, and that one-dimensional drainage takes place through the upper layer with hydraulic conductivity  $k$ , then the time scale for excess pore pressure dissipation is in the order of  $t \approx S/k$ . Despite the limitations of this simple model, measured and predicted values are in the same order of magnitude of hours to days (using the range in hydraulic conductivity listed in Table 3). A more refined analysis should take into consideration the effectively higher hydraulic conductivity of the upper layer in successive blast events as the number of perforations increases. Thus, the site time scale decreases as the number of blasting events and boreholes increase.

### Summary and Conclusions

A blast densification field experiment was conducted involving four blasting events at the same site in a period of 8 months. This case history involved extensive laboratory studies, field characterization, and detailed field monitoring. The main observations related to the process of blast densification follow:

- The amount of settlement decreased as the number of blasting events increased, asymptotically approaching the “terminal density” that corresponds to the imposed blast densification event; many blasting-drainage events may be required to attain the terminal density for this process.
- Blasting may be designed to restrict its impact to layers of interest. Surface settlement extends beyond the blasted area by about the blasting depth in each direction in this case study. The thickness and stiffness of the upper layer will change the area of influence.

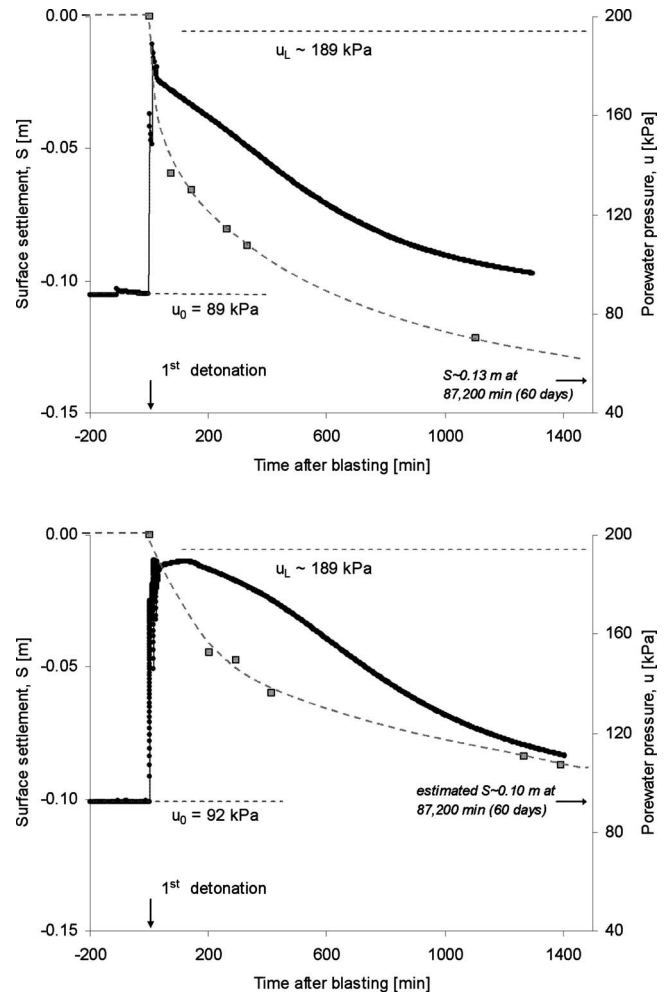


**Fig. 13.** Settlement (squares) and pore pressure dissipation (solid lines)—third and fourth blast events (measurements at the center of the test site—P2)

- The blasting sequence had a relatively small effect on shear induced movements and the settlement that followed. This observation is based on surface vibrations during blasting and postblasting subsurface settlements; further studies are required.
- Detonation delays extended the duration of imposed motion. It was very difficult to estimate optimal time delays, in part due to the complex induced deformation modes and the nonlinear evolution of the formation during the blasting sequence. Both constructive or destructive interferences develop in the field.
- Blast-induced densification is not an instantaneous phenomenon. Data and analyses indicate that the duration of settlement is related to the time scale for early drainage of fluids, resedimentation, drainage of excess pore pressure as the skeleton deforms with the increase in effective stress, and secondary settlement effects, which do not involve excess pore pressure dissipation.
- Penetration testing may fail to exhibit ground improvement following blast densification in sands that are initially very loose, or when the needed aging time exceeds the allocated construction time. In this field study, a clear increase in tip resistance was detected 2 years after the last of four blasting-drainage events.
- Surface settlement using standard surveying techniques, sub-

surface deformation assessment, and subsurface pore fluid pressure monitoring provide valuable, real-time indicators of the soil response to the blasting events, enhance the understanding of blast densification, and can be used for blast design optimization, i.e., charge size, spacing, detonation delays.

Additional observations related to monitoring and quality control follow:

- GPR and subsurface deformation data provided complementary information in this study. Both measurements confirmed the limited strains that developed in the upper soil layers. GPR penetration depth may limit its applicability to deep blasting, or in high conductivity surface layers such as in this study (clayey soils or salt water). Preblast laboratory measurements of soil electrical conductivity can be used to estimate GPR penetration depths.
- Vibration monitoring can be used to assess the implementation of delays, the generated vibration modes and shear motion, the development of constructive/destructive interferences due to time delays, propagation velocity in the far field, the attenuation of “source vibration,” and the level of vibrations in relation to potential damage to neighboring structures.

## Acknowledgments

Funding for this study was provided by the National Science Foundation, the Mid-America Earthquake Center, GeoSyntec Consultants Inc., and the Goizueta Foundation. A. Palomino and J. S. Lee performed some laboratory tests. T. S. Yun, F. Santamarina, R. Kulasingam, and G. Hebelier participated in different parts of the study.

## Notation

The following symbols are used in this paper:

- $a_n$  = CPT net area ratio obtained from triaxial calibration;
- $C$  = concentrated charge (in kg);
- $C_c$  = compression coefficient (odometer);
- $C_{cur}$  = curvature coefficient;
- $C_r$  = recompression coefficient (odometer);
- $C_u$  = uniformity coefficient;
- $D_{10}$  = effective size: equivalent sieve size that 10% of the total soil mass can pass through;
- $D_{30}$  = equivalent sieve size that 30% of the total soil mass can pass through;
- $D_{50}$  = mean size: equivalent sieve size that 50% of the total soil mass can pass through;
- $D_{60}$  = equivalent sieve size that 60% of the total soil mass can pass through;
- $D_R$  = relative density;
- $E_1$  = energy input attenuation;
- $e$  = void ratio;
- $e_0$  = initial void ratio;
- $e_{max}$  = maximum void ratio;
- $e_{min}$  = minimum void ratio;
- $f_s$  = sleeve friction;
- $f_1, f_2, f_r$  = bandwidth and resonance frequencies;
- $G_s$  = specific gravity of solids;
- $H$  = thickness of the layer treated by blast densification;

- $H_b$  = minimum distance from ground surface to top of charge (in m);
- HN = Hopkinson’s number [as defined by Ivanov (1967)];
- $k$  = hydraulic conductivity;
- $L_c$  = charge length (in m);
- $M$  = explosive charge mass (in kg);
- NM = normalized explosive charge mass [as defined by Dembicki et al. (1992)];
- $Q$  = charge loading density (in kg/m);
- $q_{1,f}$  = CPT final normalized tip resistance;
- $q_t$  = CPT corrected tip resistance;
- $q_c$  = measured tip cone resistance;
- $R$  = effective radius in plan (in m) = 1/2 grid spacing  $s$ ;
- $R_{vi}$  = minimum vector distance from charge to a point in the soil mass (in m);
- $S$  = surface settlement;
- $S_\infty$  = terminal settlement;
- $s$  = spacing (or maximum grid pattern);
- $u$  = pore water pressure;
- $u_b$  = CPT shoulder pore-water pressure;
- $u_i$  = displacement in the  $i$ th direction (i.e.,  $x$ -,  $y$ -, or  $z$ -directions);
- $u_L$  = pore pressure for full liquefaction;
- $w$  = water content;
- $z$  = depth (origin at ground surface);
- $z_w$  = ground water table depth;
- $\alpha$  = convergence decay of settlement;
- $\alpha_{vs}$  = shear wave velocity of the soil at 1 kPa confinement in  $V_s = \alpha_{vs}(\sigma'_{v0}/1 \text{ kPa})^{\beta_{vs}}$ ;
- $\beta_{vs}$  = shear wave velocity fitting parameter in  $V_s = \alpha_{vs}(\sigma'_{v0}/1 \text{ kPa})^{\beta_{vs}}$ ;
- $\gamma$  = unit weight;
- $\sigma_{fluid}$  = pore fluid electrical conductivity;
- $\sigma'_{v0}$  = effective vertical stress; and
- $\phi_{cs}$  = critical state friction angle.

## References

- Al-Qasimi, E. M. A., Charlie, W. A., and Woeller, D. J. (2005). “Canadian liquefaction experiment (CANLEX): Blast-induced ground motion and pore pressure experiments.” *Geotech. Test. J.*, 28(1), 9–21.
- Ashford, S. A., Rollins, K. M., and Lane, D. (2004). “Blast-induced liquefaction for full-scale foundation testing.” *J. Geotech. Geoenviron. Eng.*, 130(8), 798–806.
- Byrne, P. M., et al. (2000). “CANLEX full-scale experiment and modeling.” *Can. Geotech. J.*, 37(3), 543–562.
- Charlie, W. A., Rwebyogo, M. F. J., and Doehring, D. O. (1992). “Time-dependent cone penetration resistance due to blasting.” *J. Geotech. Engng.*, 118(8), 1200–1215.
- Charlie, W. A., Veyera, G. E., and Abt, S. R. (1985). “Predicting blast induced pore-water pressure increases in soils.” *Civ. Eng. Practicing and Design Engineers*, 4(3), 311–328.
- Dembicki, E., Imiolek, R., and Kisielowa, N. (1992). “Soil compaction with the blasting method.” R. N. Chowdhury, ed., *Geomechanics and water engineering in environmental management*, Balkema, Rotterdam, The Netherlands, 599–622.
- Dowding, C. H., and Hryciw, R. D. (1986). “A laboratory study of blast densification.” *J. Geotech. Engng.*, 112(2), 187–199.
- Fordham, C. J., McRoberts, E. C., Purcell, B., and McLaughlin, P. (1991). “Practical and theoretical problems associated with blast densification of loose sands.” *Proc., 44th Canadian Geotechnical Conf. of the Ca-*

- nadian Geotechnical Society, 92–98.
- Gnadh, S., Dey, A., and Selvam, S. (1999). “Densification of pond ash by blasting.” *J. Geotech. Geoenviron. Eng.*, 125(10), 889–899.
- Hachey, J. E., Plum, R. L., Byrne, J., Kilian, A. P., and Jenkins, D. V. (1994). “Blast densification of a thick, loose debris flow at Mt. St. Helen’s, Washington.” *Proc., Vertical and Horizontal Deformations of Foundations and Embankments, Geotechnical Special Publication No. 40*, 502–512.
- Hall, C. E. (1962). “Compacting a dam foundation by blasting.” *J. Soil Mech. and Found. Div.*, 88(3), 33–51.
- Imiolek, R. (1992). “Compaction of water-saturated soils by blasts from elongated charges (translated from Russian).” *Osnovaniya, Fundamenty i Mekhanika Gruntov*, 29(4), 24–26.
- Ivanov, P. L. (1967). “Compaction of noncohesive soils by explosions (translated from Russian 1972).” *National Technical Information Service Rep. No. TT 70-57221*, U.S. Dept. of Commerce, Springfield, Va.
- Ivanov, P. L. (1983). “Prediction and control techniques to compact loose soils by explosions.” *Proc., 8th European Conf. on Soil Mechanics and Foundation Engineering*, 253–254.
- Jefferies, M. G., and Rogers, B. T. (1993). “Discussion of ‘Time-dependent cone penetration resistance due to blasting’ by W. A. Charlie, M. F. J. Rwebyogo, and D. O. Doehring.” *J. Geotech. Engrg.*, 119(2), 2008–2012.
- Kayen, R. E., Barnhardt, W. A., Ashford, S., Rollins, K., Minasian, D. L., and Carkin, B. A. (2005). “High-resolution crosshole radar tomography: Application to liquefaction-induced changes in soil on Treasure Island.” *USGS-PP 1658*.
- Kulhawy, F. H., and Mayne, P. W. (1990). “Manual on estimating soil properties for foundation design.” Electric Power Research Institute, Palo Alto, Calif.
- La Fosse, U. (2002). “Improvements by deep blasting: Marine Corps Reserve Training Center.” Westover Air Reserve Base.
- Lee, J. S., and Santamarina, J. C. (2007). “Seismic monitoring short-duration events: Liquefaction in 1 g models.” *Can. Geotech. J.*, 44(6), 659–672.
- Lyman, A. K. (1942). “Compaction of cohesionless foundation soils by explosives.” *Trans. Am. Soc. Civ. Eng.*, 107, 1330–1348.
- Minaev, O. P. (1993). “Effective compaction of water-saturated soils by blasting.” *Osnovaniya, Fundamenty i Mekhanika Gruntov*, 30(2), 17–19.
- Mitchell, J. K. (1981). “Soil improvement: State-of-the-art.” *Proc., 10th Int. Conf. on Soil Mechanics and Foundation Engineering (10th IC-SMFE)*, 509–565.
- Mitchell, J. K. (2008). “Aging of sand—A continuing enigma?” *Proc., 6th Int. Conf. on Case Histories in Geotechnical Engineering*, SOAP 11, 1–21.
- Mitchell, J. K., and Gallagher, P. M. (1998). “Guidelines for ground improvement of civil works and military structures and facilities.” *Publication No. ETL 1110-1-185*, U.S. Army Corps of Engineers, Washington, D.C.
- Narin van Court, W. A. (1997). “Investigation of the mechanisms and predictive methodologies for explosive compaction.” *Civil and environmental engineering*, Univ. of California at Berkeley, Berkeley, Calif.
- Narin van Court, W. A. (2003). “Explosive compaction revisited: New guidance for performing blast densification.” *Proc., SARA 2003, 12th Panamerican Conf. on Soil Mechanics and Geotechnical Engineering and 39th U. S. Rock Mechanics Symp.*, P. J. Culligan, H. H. Einstein, and A. J. Whittle, eds., 1725–1730.
- Narin van Court, W. A., and Mitchell, J. K. (1994). “Soil improvement by blasting.” *J. Explosives Eng.*, 12(3), 34–41.
- Narin van Court, W. A., and Mitchell, J. K. (1998). “Investigation of predictive methodologies for explosive compaction.” *Geotechnical Special Publication No. 75*, ASCE, Reston, Va., 639–653.
- Narsilio, G. A. (2006). “Spatial variability and terminal density: Implications in soil behavior.” School of Civil and Environmental Engineering, Georgia Institute of Technology, Atlanta.
- Narsilio, G. A., and Santamarina, J. C. (2008). “Terminal densities.” *Geotechnique*, 58(8), 669–674.
- Prugh, B. J. (1963). “Densification of soils by explosive vibrations.” *J. Constr. Div.*, 89(1), 79–100.
- Raju, V. R., and Gudehus, G. (1994). “Compaction of loose sand deposits using blasting.” *Proc., 13th Int. Conf. on Soil Mechanics and Foundation Engineering*, 1145–1150.
- Richart, F. E., Hall, J. R., and Woods, R. D. (1970). *Vibrations of soils and foundations*, Prentice-Hall, Englewood Cliffs, N.J.
- Robertson, P. K., et al. (2000). “CANLEX project: Summary and conclusions.” *Can. Geotech. J.*, 37(3), 563–591.
- Rogers, B. T., Graham, C. A., and Jefferies, M. G. (1990). “Compaction of hydraulic fill sand in Molikpaq core.” *Proc., Prediction and Performance in Geotechnique, 43rd Canadian Geotechnical Conf.*, 567–575.
- Solymar, Z. V. (1984). “Compaction of alluvial sands by deep blasting.” *Can. Geotech. J.*, 21, 305–321.
- Terzaghi, K., Peck, R. B., and Mesri, G. (1996). *Soil mechanics in engineering practice*, Wiley, New York.
- van Impe, W. F. (1989). *Soil improvement techniques and their evolution*, Brookfield Publishers, Rotterdam, The Netherlands.
- Wild, P. A. (1961). “Tower foundations compacted with explosives.” *Electr. World*, 66, 36–38.